Journal of Power Sources 271 (2014) 522–529

Contents lists available at ScienceDirect

Journal of Power Sources

journal homepage: www.elsevier.com/locate/jpowsour

Egg derived nitrogen-self-doped carbon/carbon nanotube hybrids as noble-metal-free catalysts for oxygen reduction

Jian Zhang, Siyu Wu, Xu Chen, Mu Pan, Shichun Mu*

State Key Laboratory of Advanced Technology for Materials Synthesis and Processing, Wuhan University of Technology, Wuhan 430070, China

HIGHLIGHTS

- Novel non-noble metal catalysts for ORR are obtained using eggs as N and C sources.
- The catalyst shows a catalytic activity comparable to Pt/C in alkaline media.
- The catalyst has superior stability and fuel tolerance than Pt/C in alkaline media.
- It provides a promising alternative to noble metal catalysts by using eggs.

GRAPHICAL ABSTRACT

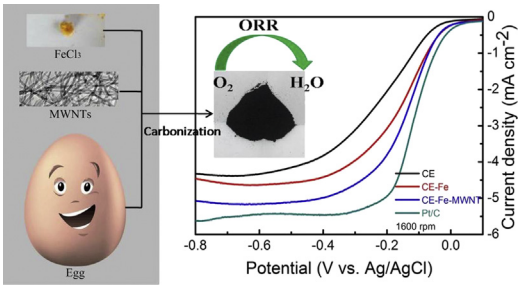

ARTICLE INFO

Article history:
Received 26 June 2014
Received in revised form
26 July 2014
Accepted 11 August 2014
Available online 21 August 2014

Keywords:
Egg
Noble-metal-free catalyst
Oxygen reduction reaction
Low temperature fuel cells

ABSTRACT

Currently, the development of nitrogen (N) doped carbon based non-precious metal ORR catalysts has become one of the most attractive topics in low temperature fuel cells. Here, we demonstrate a green synthesis route of N-self-doped carbon materials by using eggs as N sources combining with iron sources and multi-walled carbon nanotubes (CE–Fe–MWNT). After carbonized, such hybrid materials possess an outstanding electrocatalytic activity towards ORR comparable to the commercial Pt/C catalyst in alkaline media, and both superior stability and fuel (methanol and CO) tolerance than the commercial Pt/C catalyst, which provide a promising alternative to noble metal catalysts by using abundant natural biological resources.

1. Introduction

Pt-based catalysts represent a state of the art in the electrocatalysis of oxygen reduction reaction (ORR) for low temperature fuel cells (LTFCs) which can convert chemical energy directly into electricity without combustion processes and with high energy conversion efficiencies [1]. However, Pt is both expensive and scarce, greatly limiting its widespread implementation in LTFCs. Besides, Pt-based catalyst still suffers from serious intermediate tolerance, such as carbon monoxide (CO) poisoning and methanol crossover as well as poor stability in an electrochemical environment [2–6]. Consequently, considerable research efforts have been devoted to developing a high performance noble-metal-free catalyst (NMFC) with earth-abundant elements.

Carbon is a very common element, which widely exists in the Earth. The heteroatom doped carbon materials not only exhibit high catalytic activity and long-term stability, but also excellent CO and methanol poisoning resistances [1,7–9]. Hitherto, investigating heteroatom doped carbon catalysts for ORR becomes one of the hottest topics in LTFCs. As reported, the carbon based catalysts have been achieved by doping various heteroatoms (such as N, B, P, S, Fe or Co) [3,7,10–13]. Among them, transition metal N-doped carbon

* Corresponding author. Tel.: +86 27 87651837; fax: +86 27 87879468.
E-mail addresses: msc@whut.edu.cn, mushichun@gmail.com (S. Mu).

http://dx.doi.org/10.1016/j.jpowsour.2014.08.038
0378-7753/

materials have exhibited the best catalytic performance for ORR [7,10,14]. However, such N-containing compounds are either expensive or harmful to human health, because most of N sources always derive from expensive organic monomers containing nitrogen element or ammonia [15–17]. Therefore, the long-term development of N-doped carbon electrocatalysts with non-toxic and cheaper N sources is highly desirable.

Eggs are natural and widely available biological materials with abundant heteroatoms (C, H, O, N, et al.). It can take place of conventional N-containing organic compounds or ammonia to develop the N-doped carbon catalyst, meeting the requirements for nontoxic and inexpensive properties. In this paper, the egg is employed as a N source mixing with the transition metal iron and multi-walled carbon nanotubes (MWNTs). After cooked, dried and carbonized at high temperatures and followed post-treatments (PTs) including ball milling, acid leaching and the second heat treatment (as shown in Fig. 1), the CE–Fe–MWNT hybrid material is obtained. Here the highly graphitized MWNTs provide a robust matrix for hosting the active sites due to its superior electrical conductivity and excellent mechanical and chemical stability. The electrochemical characterization shows that this hybrid material possesses an outstanding electrocatalytic ORR activity in alkaline media, and both superior stability and fuel (methanol and CO) tolerance compared to the commercial Pt/C catalyst. This work shows a good example for taking advantage of the abundant resources provided by natural biological materials as a promising alternative for costly Pt-based catalysts.

2. Experimental section

2.1. Materials

Eggs were purchased from local super market. The multi-walled carbon nanotubes (MWNTs, with ca. 80 nm in diameter and ca. 110 $m^2 g^{-1}$ in surface area) were treated in an aqueous HCl solution for 24 h to remove the potential metal impurities. Ferric chloride ($FeCl_3 \cdot 6H_2O$) and potassium hydroxide (KOH) were purchased from Sinopharm Chemical Reagent, and Nafion solution (5 wt %) was obtained from Sigma–Aldrich. All the chemicals were used as delivered without further treatment. Ultra pure water was obtained from a Lab. ultra pure water filter system with a resistivity $\geq$18 MΩ cm^{-1}. Rotating disk electrodes of glassy carbon (RDE, 5 mm in diameter) were purchased from Tianjin Aida Hengsheng Tech. Co., China.

2.2. Material syntheses

Eggs were diluted with an equal amount of water. And then 0.1 mol L^{-1} $FeCl_3$ mixing with MWNT solution was added dropwise to the above suspension and kept stirring for 2 h (Fe: MWNT: egg = 0.1: 0.2: 10, wt. %). The mixture was cooked in a water bath (100 °C, 2 h), and then dried in an air-circulating oven at 80 °C to obtain the precursor. The precursor was carbonized at 900 °C in an inert atmosphere. Temperature settings were as follows: the precursor was performed at 200 °C for 0.5 h at a heating rate of 2 °C min^{-1} in an inert atmosphere, subsequently it was performed at 900 °C for 2 h at a heating rate of 5 °C min^{-1} in an inert atmosphere, and then the sample was cooled under the same atmosphere from 900 °C to 60 °C. After that, the black carbon was transferred into a milling tank and grinded on a planetary ball mill (Nanjing Chishun Science & Technology Co., Ltd. PM) for 4 h at 250 rpm. The resulting black carbon powder was pre-leached in 0.5 M H_2SO_4 at 80 °C for 8 h to remove unstable and inactive species from the catalyst, followed by thoroughly washed in de-ionized water and absolute ethyl alcohol, and then dried at 80 °C under vacuum. Finally, the product was heat-treated again at 900 °C for 2 h at a heating rate of 5 °C min^{-1} in nitrogen atmosphere to obtain the CE–Fe–MWNT catalyst. The specific synthesis process of CE–Fe–MWNT catalyst is shown in Fig. 1.

2.3. Physical and chemical characterizations

The morphology and structure of the samples were further analyzed using JSM-7100F field emission scanning electron microscope (FESEM) and JEM-2100F high-resolution transmission electron microscopy (TEM). Nitrogen adsorption–desorption isotherms were recorded at 78 K with a Micromeritics ASAP 2020 Brunauer Emmett Teller (BET) analyzer. The electronic structure of surfaces for the catalyst was performed using VG-Multi-lab2000 X-ray photoelectron spectroscopy (XPS). Accurate iron content of these catalysts was performed using inductively coupled plasma-atomic emission spectrometry (ICP-AES). Raman spectroscopy

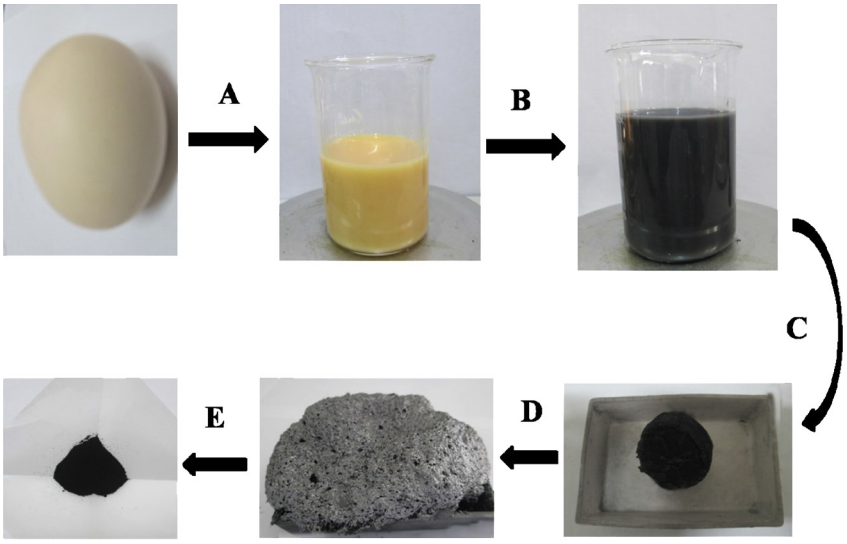

Fig. 1. Schematic of the synthesis process of CE–Fe–MWNT catalyst. (A) Cracking the egg and mixing with water. (B) Adding $FeCl_3$ mixing with MWNT solution. (C) Cooking and drying it. (D) The precursor was carbonized in an inert atmosphere. (E) The post-treatment including ball milling, acid leaching and the second heat treatment.

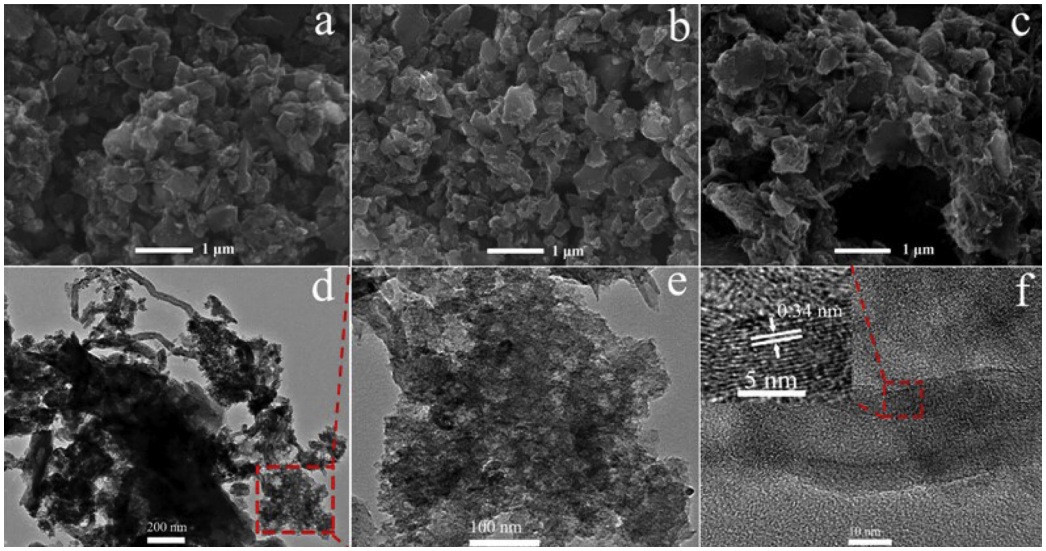

Fig. 2. FESEM images (a–c) of CE, CE–Fe and CE–Fe–MWNT, and the different magnification TEM image of CE–Fe–MWNT (d–f), inset: MWNT.

was carried out on a Renishaw using the Ar ion laser with an excitation wavelength of 514.5 nm.

2.4. Electrochemical characterizations

ORR activity of the catalyst was evaluated on an electrochemical workstation at room temperature using a three-electrode electrochemical cell. Counter and reference electrodes were a platinum wire and an Ag/AgCl (saturated KCl solution) electrode, respectively. Working electrode was constructed with a glassy carbon disk electrode (0.2 cm^2) coated with the catalyst layer. To prepare the working electrode, a homogeneous catalyst ink was made by mixture of 5.0 mg catalyst, 25 μL Nafion ionomer solution (5 wt%, DuPont) and 0.475 mL ultra pure water. The working electrode was prepared by loading 0.3 mg cm^{-2} sample on a glassy carbon electrode. As a benchmark, the commercial Pt/C (20 wt%, JM) catalyst was also spread onto the surface of a glassy carbon disk electrode in a similar way, the Pt loading was 20 μg Pt cm^{-2}.

ORR activity was carried out using rotating disk electrode (RDE) technique by linear sweep voltammetry (LSV) in the potential range of −0.8 to 0.2 V (vs. Ag/AgCl) with a scan rate of 5 mV s^{-1} at different rotation rate from 400 to 2000 rpm in an O_2-saturated 0.1 M KOH solution. The tolerance of the catalysts were investigated by LSV and current vs time (i–t) chronoamperometric

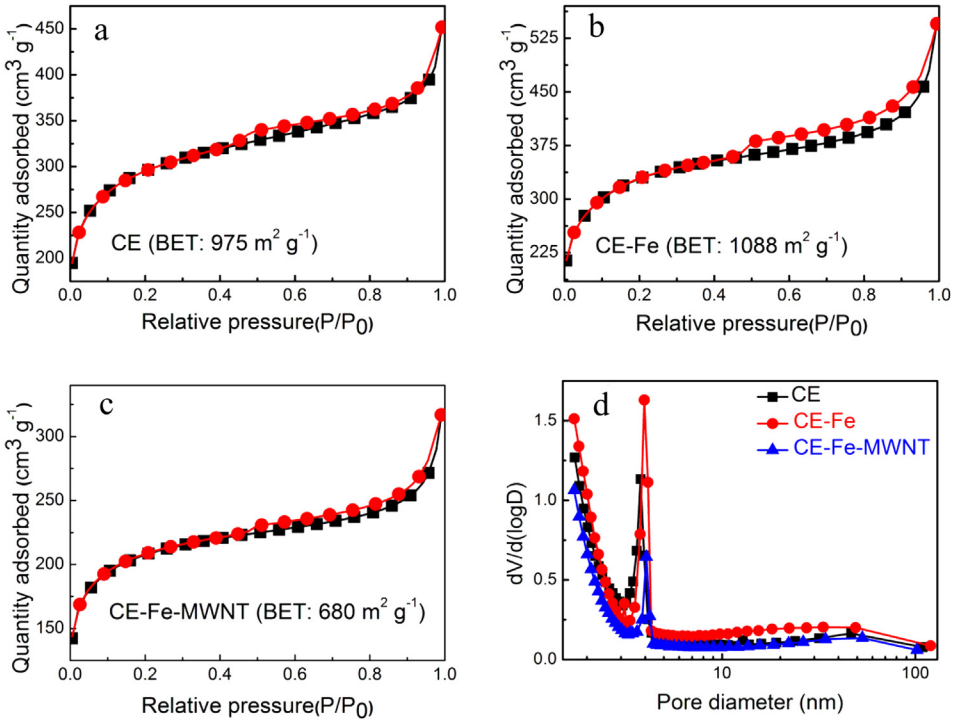

Fig. 3. N_2 adsorption–desorption isotherms (a–c) and the pore size distribution (d) of CE, CE–Fe and CE–Fe–MWNT catalysts, respectively.

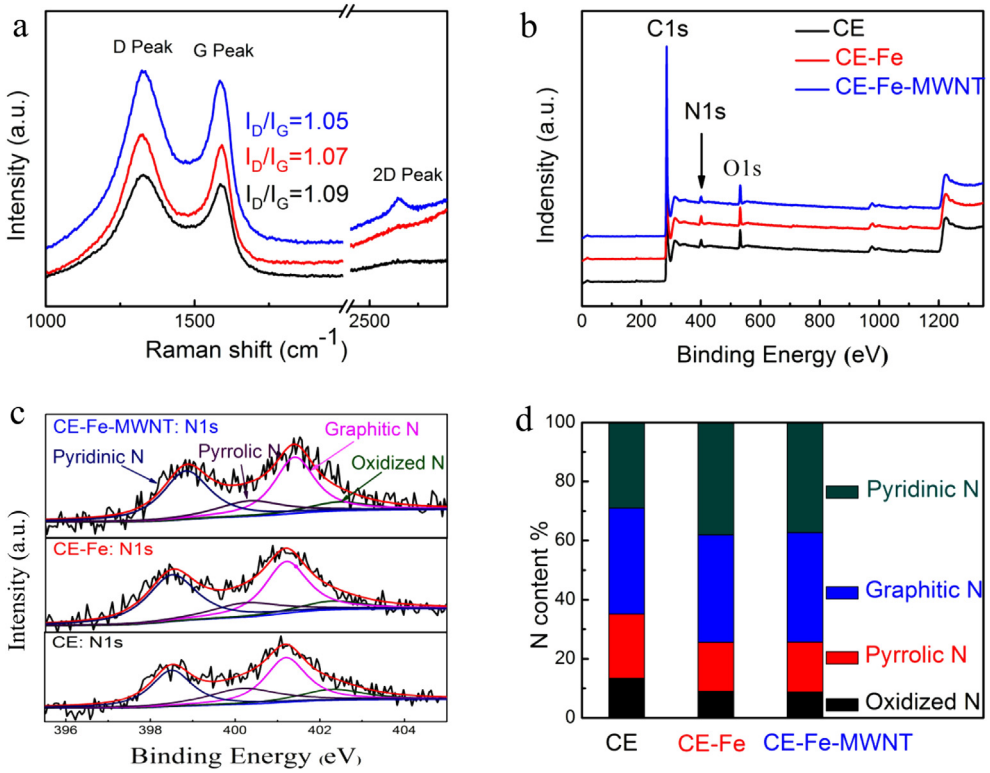

Fig. 4. Raman (a) and XPS (b) spectrum of CE, CE–Fe and CE–Fe–MWNT, respectively; N 1s fitted results and (c) and relative ratio of N content (d) of CE, CE–Fe and CE–Fe–MWNT, respectively.

response during a constant potential at −0.5 V in (O_2-saturated, O_2 + CO and O_2 + 3 M CH_3OH) 0.1 M KOH solution. ORR stabilities of the catalysts were investigated by *i–t* chronoamperometric response of the CE–Fe–MWNT and Pt/C during a constant potential at −0.35 V at a rotation rate of 1600 rpm in O_2-saturated 0.1 M KOH. After *i–t* chronoamperometric response, the ORR steady-state polarization measurement was conducted in O_2-saturated 0.1 M KOH electrolyte with scanning rates of 5 mV s^{-1} and rotation rate at 1600 rpm. The electrochemical impedance spectroscopy (EIS) measurements were performed under open circuit potential with an excitation signal of 5 mV at frequency ranges of 100 kHz to 0.1 Hz. The onset potential (E_{onset}) was defined as the potential at which the ORR current is 5% of the diffusion-limited current, the half-wave potential ($E_{1/2}$) was defined as the potential at which the ORR current is 50% of the diffusion-limited current [18].

3. Results and discussion

3.1. Morphology and structure

Fig. 1 shows the synthesis process of the CE–Fe–MWNT hybrid. The mixed solution of the transition metal iron and MWNTs was added into the egg suspension to obtain the precursor. And then the as-prepared precursor was cooked in a water bath (100 °C, 2 h), dried in an air-circulating oven at 80 °C and carbonized at high temperatures in an inert atmosphere to obtain a very fluffy and porous carbon material. In this step, the slow heating procedure and thermal insulation for 0.5 h at 200 °C (step D in Fig. 1) was very important to increase the catalyst surface area, because in this case the biomass materials would swell besides partially carbonized. [19,20]. It was similar to making bread. Subsequently, the CE–Fe–MWNT hybrid was obtained through a series of post-treatment (PTs), which plays a crucial role in promoting the electrochemical performance of the catalyst, as detailed in the previous work [10]. For comparison, the samples of CE (without iron and MWNTs), Fe–MWNT (without eggs) and CE–Fe (without MWNTs) were also obtained by the similar way.

Morphologies of the catalysts were investigated by means of the FESEM. Fig. 2a and b shows nearly identical morphologies in CE and CE–Fe catalysts. However, Fig. 3a and b shows the BET surface area of CE–Fe (BET: 1,088 m^2 g^{-1}) is higher than that of CE (BET: 975 m^2 g^{-1}). Some iron oxides were formed in CE–Fe at high temperatures (Fig. 1, step D), however most of them can be removed by acid leaching and subsequently formed a number of pores, leading to high surface area. Fig. 2c shows the carbonized egg can be well combined with MWNTs, which can also be observed by TEM in Fig. 2d. In addition, the high-resolution TEM image exhibits a porous structure of carbon in CE–Fe–MWNT (Fig. 2e) where

Table 1
Surface atomic concentrations of C, N, O and the relative ratio of different types of N contents of CE, CE–Fe and CE–Fe–MWNT, the trace content of iron by ICP-AES.

Sample	C (at%)	O (at%)	N (at%)	Oxidized N (%)	Graphitic N (%)	Pyrrolic N (%)	Pyridinic N (%)	Fe (wt%)
CE	89.77	7.30	2.93	13.01	34.15	16.65	36.17	0.297
CE–Fe	92.82	4.38	2.70	8.88	33.70	12.22	45.18	0.829
CE–Fe–MWNT	94.86	2.98	2.16	8.56	34.12	12.35	44.96	0.763

carbon is in close contact with the MWNTs (Fig. 2f). However, Fig. 3c shows CE–Fe–MWNT has lower surface area (BET: 680 m^2 g^{-1}) than CE and CE–Fe samples due to the addition of MWNTs with relatively low surface area (BET: 110 m^2 g^{-1}). In addition, Fig. 3d shows the pore distribution of CE, CE–Fe and CE–Fe–MWNT, demonstrating a larger number of mesopores within catalysts. The high surface area can make the catalyst possess high density of active sites, and the mesoporous structure benefits to the diffusion of ORR related species, which are both conducive to improve ORR activities [11,20,21].

Raman spectrum was used to investigate the carbon structure of catalyst. There are two peaks at approximately 1340 cm^{-1} and 1590 cm^{-1}, corresponding to the D peak and G peak, respectively [22,23]. As shown in Fig. 4a, the ratio of I_D/I_G successively decreases from CE, CE–Fe to CE–Fe–MWNT, indicating the degree of graphitization sequentially increases [22]. Higher degree of graphitization of CE–Fe over CE is owing to the catalytic function of iron which accelerates the graphitization substantially at a lower temperature (600–900 °C) [7,8,16]. The iron species can interact with amorphous carbon particles, leading to a surface rearrangement and simultaneously coordinating with N and carbon in the interstices of the graphitic layers within micropores, which is very beneficial to improve the ORR activity [16,23]. Among the samples, the highest degree of graphitization of CE–Fe–MWNT is caused by the graphitic structure of MWNTs. The presence of 2D peak at ca. 2650 cm^{-1} can further confirm the change of the graphitic structure in the catalyst. XPS measurements were carried out to get a full understanding of the surface composition of the catalyst. Fig. 4b and Table 1 shows CE, CE–Fe and CE–Fe–MWNT catalysts were predominantly composed of C, N and O elements. ICP-AES test results show the trace content of iron in CE, CE–Fe and CE–Fe–MWNT (Table 1). These results indicate that most of transition metal iron in the catalysts was leached out after the acid treatment, and only a few part of it chelated with amino acid and incorporated in the carbon matrix (see below) can be preserved even after washed with concentrated proton acid [24]. Analyses of N 1s spectrum reveal the presence of oxidized N (ca. 402.3 eV), graphitic N (ca. 401.1 eV), pyrrolic N (ca. 400.5 eV) and pyridinic N (ca. 398.2 eV) [7,10,16,17,25]. Although the overall N content sequentially decreases with the order of CE, CE–Fe and CE–Fe–MWNT, the relative ratio of pyridinic and graphitic N in both CE–Fe and CE–Fe–MWNT is higher than CE (Fig. 4d), because iron can promote the formation of the pyridinic and graphitic N at elevated temperatures, which is consistent with the earlier work [23]. It has been reported that graphitic N can greatly increase the limiting current density, and pyridinic N can improve the onset potential and wettability, while other N species such as pyrrolic N or oxidized N have little effect on the electrochemical performance of carbon materials [24,26].

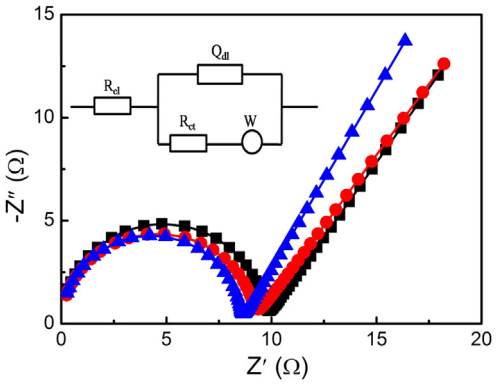

Fig. 6. EIS of CE, CE–Fe and CE–Fe–MWNT, inset: the equivalent circuit, where R_{el} is solution resistance, R_{ct} is charge transfer resistance, W is Warburg element, Q_{dl} is double layer capacitance.

3.2. Electrocatalytic activity for ORR

To investigate the ORR performance, linear sweep voltammetry (LSV) measurements were performed on a rotating disk electrode (RDE) in O_2-saturated 0.1 M KOH solution. Fig. 5 shows the E_{onset} and $E_{1/2}$ positively shift with the order of Fe–MWNT, CE, CE–Fe and

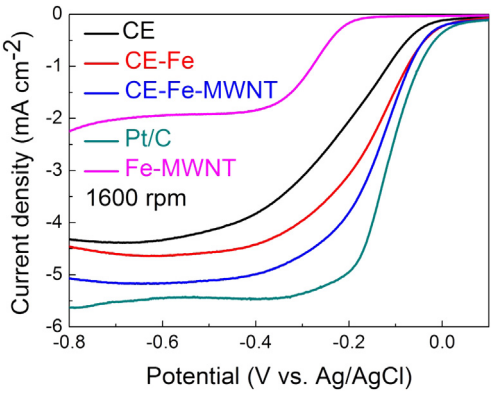

Fig. 5. LSV curves for CE, CE–Fe, Fe–MWNT, CE–Fe–MWNT and commercial Pt/C catalysts in O_2-saturated 0.1 M KOH solution with scanning rates of 5 mV s^{-1} and the rotation rate at 1,600 rpm.

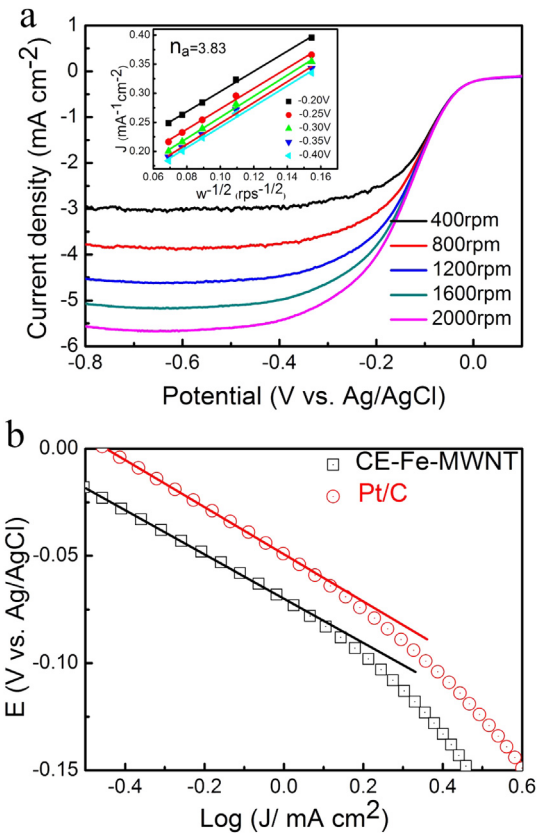

Fig. 7. ORR polarization curves for CE–Fe–MWNT at different rotating rates in O_2-saturated 0.1 M KOH solution with scanning rates of 5 mV s^{-1} (a), inset: K–L plots; Tafel plots for CE–Fe–MWNT and Pt/C extracted from Fig. 4(b).

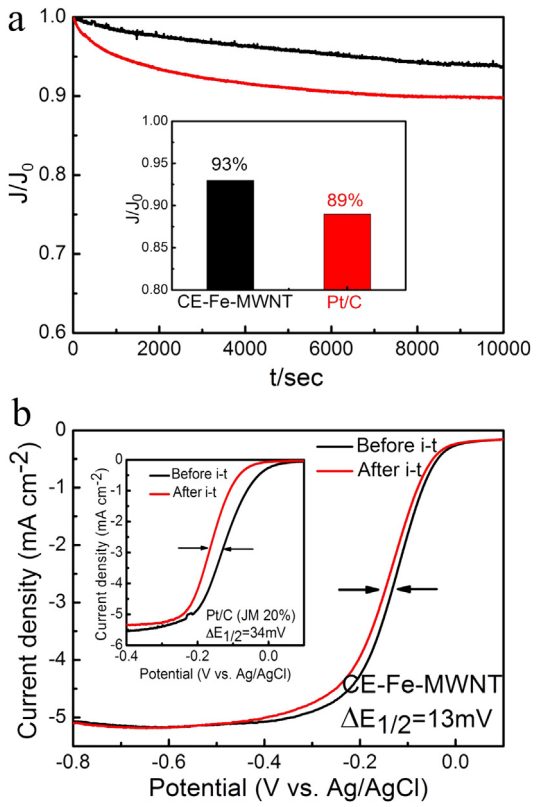

Fig. 8. The current vs. time (i–t) chronoamperometric responses of CE–Fe–MWNT and Pt/C in O_2-saturated during a constant potential at −0.35 V and a rotation rate of 1,600 rpm; inset: the ratio of the J/J_0 (a); the stability of CE–Fe–MWNT is symbolized by $\Delta E_{1/2}$ before and after i–t test, inset: Pt/C (b).

CE–Fe–MWNT, and the ORR activity of CE–Fe–MWNT ($E_{onset} = -0.007$ V, $E_{1/2} = -0.133$ V) is only slightly lower than that of the commercial Pt/C (JM 20 wt%) catalyst. In addition, the electro-catalytic activity of this hybrid catalyst is comparable to the reported N-doped graphene or carbon nanotubes by using N-containing monomers or polymers as N sources. A detailed comparison of electro-catalytic activities of above-mentioned materials for ORR is shown in Table S1 (Supporting information, SI). The higher ORR activity of CE–Fe than that of CE is mainly due to the addition of iron, because the egg itself with lower content of iron (0.015 wt%) detected by ICP-AES, is unable to form sufficient active sites during the high temperature treatment. When transition metal iron was added into eggs, it would chelate with the amino acid in eggs to form a transition metal chelate compounds, which is similar to the porphyrin or phthalocyanine [4,16,24]. Such compounds have high ORR activity after high temperature treatments in an inert atmosphere [1,27]. Although ICP-AES test results show the presence of a trace iron in the catalyst after the acid treatment, such extremely small amount of iron residuals can further facilitate the formation of catalytic sites and boost the ORR activity of the catalyst [24]. In spite of the role of iron has been a long-term debated topic that whether iron is necessary for improving the activity or not [3,24,28]. The current wisdom is that both iron and N are needed, because the calculation results by the density functional theory indicate the existence of the transition metal that plays a pivotal role in initializing the ORR activity of the catalyst [24,29]. CE–Fe and CE–Fe–MWNT catalysts possess more iron residuals, leading to better ORR activity than CE. In addition, the addition of iron can promote the graphitization of carbon, increasing the electron conductivity which improves the ORR activity [3,4,24]. Fig. 6 shows Nyquist plots of EIS of the catalyst. According to the equivalent circuit (inset of Fig. 6), the fitted results reveal that CE–Fe–MWNT has the lowest charge transfer resistance (8.6 Ω cm^{-2}) compared to

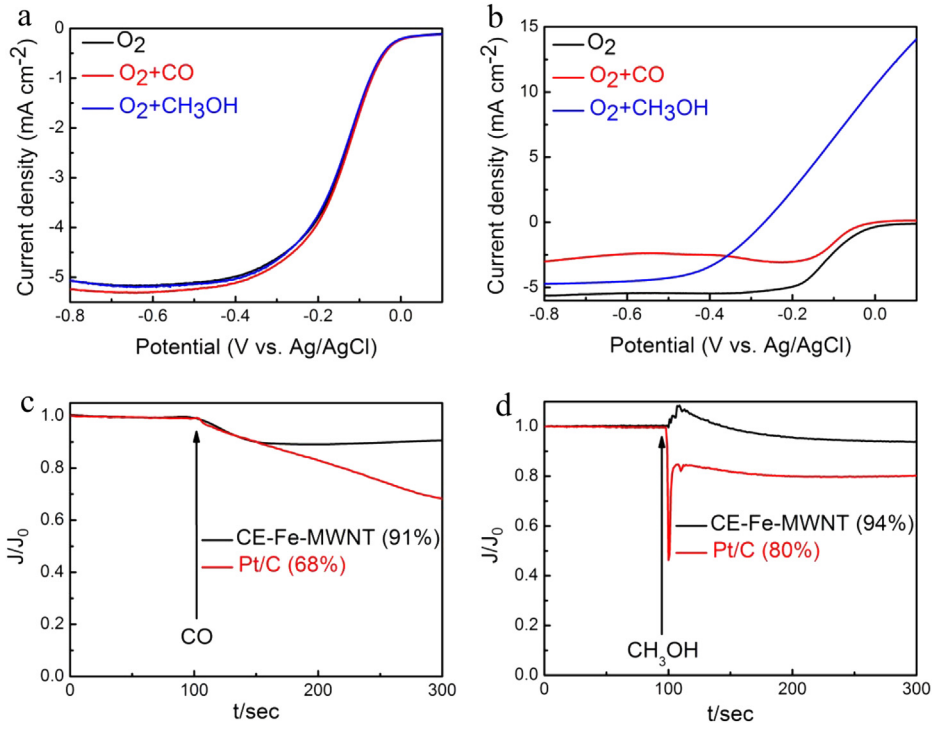

Fig. 9. Tolerance of CE–Fe–MWNT and Pt/C. LSVs of CE–Fe–MWNT (a) and Pt/C (b) in O_2-saturated, CO and O_2-saturated (V_{CO}/V_{O_2} = 10%), 3 M methanol O_2-saturated 0.1 M KOH with scan rate of 5 mV s^{-1} at 1600 rpm; i–t chronoamperometric responses of CE–Fe–MWNT and Pt/C in CO and O_2-saturated (V_{CO}/V_{O_2} = 10%) (c) and 3 M methanol O_2-saturated (d) during a constant potential at −0.5 V at a rotation rate of 1,600 rpm in 0.1 M KOH.

CE (9.9 Ω cm^{-2}) and CE–Fe (9.4 Ω cm^{-2}). Therefore, compared to CE–Fe, the ORR activity of CE–Fe–MWNT can be further improved due to the high degree of graphitization of MWNTs constructing an excellent charge transfer channel [1,16,30]. This suggests that the ORR activity of the catalyst not only depends on the amount and chemical state of active sites, but also appreciably affected by electron transport [31,32].

ORR polarization curves for CE–Fe–MWNT were further tested at various rotating rates from 400 to 2000 rpm (Fig. 7a). The inset of Fig. 7a shows the Koutecky–Levich (K–L) [11,13] plots at a variety of potentials for CE–Fe–MWNT. The K–L equation as below:

$$\frac{1}{J} = \frac{1}{J_L} + \frac{1}{J_K} = \frac{1}{B\omega^{1/2}} + \frac{1}{J_K} \quad (1)$$

$$B = 0.62nFC_0(D_0)^{2/3}\upsilon^{-1/6} \quad (2)$$

where J denotes the measured current density, J_K is the kinetic current density, J_L is the diffusion-limited current density, ω is the electrode rotation rate, F is the Faraday constant (96485C mol^{-1}), C_0 is the bulk concentration of O_2 (1.2×10^{-3} mol L^{-1}), D_0 is the diffusion coefficient of O_2 (1.9×10^{-5} cm^2 s^{-1}) and v is the kinetic viscosity of the electrolyte (1.0×10^{-2} cm^2 s^{-1}). The average electron transfer number (n_a) of the hybrid is 3.83 calculated by the slope (inset: Fig. 7a), which is very close to Pt/C. The high ORR activity of CE–Fe–MWNT is further supported by the small Tafel slope of 71 mV $decade^{-1}$ (Fig. 7b) which very approaches Pt/C (65 mV $decade^{-1}$), indicating a similar reaction mechanism in alkaline media [2,3,32].

The stability test of catalysts shows that Pt/C suffers from 11% loss of the current density after 10,000 s current vs. time (i–t) chronoamperometric reaction, whereas in this case CE–Fe–MWNT only exhibits 7% decrease in current density (Fig. 8a). Subsequently, the half-wave potential decay ($\Delta E_{1/2}$) of Pt/C is 34 mV before and after i–t chronoamperometric response, much higher than CE–Fe–MWNT ($\Delta E_{1/2}$ = 13 mV, Fig. 8b). We also investigated the ORR polarization curves for CE–Fe–MWNT and Pt/C catalysts before and after accelerated durability test of 5,000 cycles from −0.6 to 0 V, as shown in Fig. S1. These results have also confirmed that the hybrid material is more stable than Pt/C in alkaline media. The ORR activity of Pt/C decreases rapidly due to dissociation or detachment/aggregation of Pt nanoparticles during the continuous electrochemical oxidation of carbon supports [14,17]. The excellent stability of our catalysts can be mainly attributed to the covalent bonding of the catalytically active heteroatom to the carbon framework, unlike the physical bonding of Pt over carbon supports [16,33].

To investigate possible crossover effects, we tested the electrocatalytic selectivity of catalysts against the electro-oxidation of methanol (3 M) and carbon monoxide (CO), respectively. As shown in Fig. 9a, no activity specific to methanol or CO is observed on the hybrid material where the characteristic peaks of ORR are maintained. Whereas the electro-oxidation of methanol or CO on Pt/C seriously retards the ORR process (Fig. 9b), as indicated by the decrease of the oxygen reduction. The i–t chronoamperometric reaction also shows that the hybrid is insensitive to CO and methanol poisoning, whereas Pt/C is rapidly poisoned with dramatically decreased current density due to the blockage of active sites on Pt nanoparticles by adsorption of CO or methanol oxidation intermediate products (Fig. 9c and d) [14,34]. These results reveal our new catalyst not only has a higher catalytic selectivity toward ORR, but also has excellent stability than that of Pt/C. More importantly, considering that the cost of raw materials for preparing the hybrid material is much cheaper than that of the commercial Pt/C catalyst, it is a nice alternative to the Pt-based catalyst for fuel cells.

4. Conclusions

In summary, we employ the egg as N sources to obtain a novel N-self-doped carbon catalyst by adding transition metal iron and multi-walled carbon nanotubes. The high temperature expansion property of the biological matrix material causes the catalyst own a high surface area due to formation of larger number of nano-pores, and MWNTs provide a fast electron transfer pathway for ORR. The electrochemical tests show that the prepared hybrid catalyst possesses outstanding electrocatalytic ORR activity comparable to the commercial Pt/C catalyst in alkaline media, and significantly superior stability and immunity for methanol crossover and CO poisoning than Pt/C. Thus, we demonstrate a general approach to preparing a highly efficient and durable N-doped carbon catalyst for ORR by using abundant natural biological materials.

Acknowledgments

This work was supported financially by the National Natural Science Foundation of China (NSFC) (No. 51372186), and the National Basic Research Development Program of China (973 Program) (No. 2012CB215504).

Appendix A. Supplementary data

Supplementary data related to this article can be found at http://dx.doi.org/10.1016/j.jpowsour.2014.08.038.

References

[1] N. Daems, X. Sheng, I.F. Vankelecom, P.P. Pescarmona, J. Mater. Chem. A 2 (2014) 4085–4110.
[2] X. Sun, P. Song, Y. Zhang, C. Liu, W. Xu, W. Xing, Sci. Rep. 3 (2013) 2505.
[3] J. Liu, X. Sun, P. Song, Y. Zhang, W. Xing, W. Xu, Adv. Mater. 25 (2013) 6879–6883.
[4] R. Cao, R. Thapa, H. Kim, X. Xu, M.G. Kim, Q. Li, N. Park, M. Liu, J. Cho, Nat. Commun. 4 (2013) 2076.
[5] H. Yin, C. Zhang, F. Liu, Y. Hou, Adv. Funct. Mater. 24 (2014) 2930–2937.
[6] D. He, C. Zen, C. Xu, S. Mu, M. Pan, Langmuir 27 (2011) 5582–5588.
[7] G. Wu, K.L. More, C.M. Johnston, P. Zelenay, Science 332 (2011) 443–447.
[8] M. Lefèvre, E. Proietti, F. Jaouen, J.P. Dodelet, Science 324 (2009) 71–74.
[9] K. Gong, F. Du, Z. Xia, M. Durstock, L. Dai, Science 323 (2009) 760–764.
[10] J. Zhang, D. He, H. Su, X. Chen, M. Pan, S. Mu, J. Mater. Chem. A 2 (2014) 1242–1246.
[11] J. Wu, Z. Yang, X. Li, Q. Sun, C. Jin, P. Strasser, R. Yang, J. Mater. Chem. A 1 (2013) 9889–9896.
[12] X. Sun, Y. Zhang, P. Song, J. Pan, L. Zhuang, W. Xu, W. Xing, ACS Catal. 3 (2013) 1726–1729.
[13] Y. Hu, X. Zhao, Y. Huang, Q. Li, N.J. Bjerrum, C. Liu, W. Xing, J. Power Sources 225 (2013) 129–136.
[14] P. Zhang, X. Chen, J. Lian, Q. Jiang, J. Phys. Chem. C 116 (2012) 17572–17579.
[15] J. Maruyama, T. Hasegawa, S. Iwasaki, H. Kanda, H. Kishimoto, ACS Sustain. Chem. Eng. (2013), 2168-0485.
[16] G. Wu, C.M. Johnston, N.H. Mack, K. Artyushkova, M. Ferrandon, M. Nelson, J.S. Lezama-Pacheco, S.D. Conradson, K.L. More, D.J. Myers, J. Mater. Chem. 21 (2011) 11392–11405.
[17] H. Peng, Z. Mo, S. Liao, H. Liang, L. Yang, F. Luo, H. Song, Y. Zhong, B. Zhang, Sci. Rep. 3 (2013) 1765.
[18] L. Birry, J.H. Zagal, J.P. Dodelet, Electrochem. Commun. 12 (2010) 628–631.
[19] Z. Li, Z. Xu, X. Tan, H. Wang, C.M.B. Holt, T. Stephenson, B.C. Olsen, D. Mitlin, Energy Environ. Sci. 6 (2013) 871–878.
[20] W. Qian, F. Sun, Y. Xu, L. Qiu, C. Liu, S. Wang, F. Yan, Energy Environ. Sci. 7 (2014) 379–386.
[21] H.W. Liang, W. Wei, Z.S. Wu, X. Feng, K. Mullen, J. Am. Chem. Soc. 135 (2013) 16002–16005.
[22] S.C. Mu, H.L. Tang, S.H. Qian, M. Pan, R.Z. Yuan, Carbon 44 (2006) 762–767.
[23] G. Wu, P. Zelenay, Acc. Chem. Res. 46 (2013) 1878–1889.
[24] S. Ganesan, N. Leonard, S.C. Barton, Phys. Chem. Chem. Phys. 16 (2014) 103–109.
[25] Z. Mo, R. Zheng, H. Peng, H. Liang, S. Liao, J. Power Sources 245 (2014) 801–807.
[26] J.P. Paraknowitsch, A. Thomas, Energy Environ. Sci. 6 (2013) 2839–2855.

[27] Q. Li, R. Cao, J. Cho, G. Wu, Phys. Chem. Chem. Phys. (2014) 1463–9084.
[28] A. Serov, K. Artyushkova, P. Atanassov, Adv. Energy Mater. (2014), http://dx.doi.org/10.1002/aenm.201301735.
[29] J. Zhu, C. He, Y. Li, S. Kang, P.K. Shen, J. Mater. Chem. A 1 (2013) 14700–14705.
[30] S.H. Lim, Z. Li, C.K. Poh, L. Lai, J. Lin, J. Power Sources 214 (2012) 15–20.
[31] S. Chen, J. Duan, M. Jaroniec, S.Z. Qiao, Adv. Mater. 26 (2014) 2925–2930.
[32] G.L. Tian, M.Q. Zhao, D. Yu, X.Y. Kong, J.Q. Huang, Q. Zhang, F. Wei, Small (2014), http://dx.doi.org/10.1002/smll.201303715.
[33] M.Y. Song, H.Y. Park, D.S. Yang, D. Bhattacharjya, J.S. Yu, ChemSusChem (2014), http://dx.doi.org/10.1002/cssc.201400049.
[34] P. Zhang, B. Xiao, X. Hou, Y. Zhu, Q. Jiang, Sci. Rep. 4 (2014) 3821.